LiNbO$_3$ acousto-optical and electro-optical micromodulators

N. Courjal
nadege.bodin@univ-fcomte.fr

University of Franche-Comté, FEMTO-ST Institute, Besançon, 25000, France

M. P. Bernal

University of Franche-Comté, FEMTO-ST Institute, Besançon, 25000, France

G. Ulliac

University of Franche-Comté, FEMTO-ST Institute, Besançon, 25000, France

J. Dahdah

University of Franche-Comté, FEMTO-ST Institute, Besançon, 25000, France

S. Benchabane

University of Franche-Comté, FEMTO-ST Institute, Besançon, 25000, France

J-M. Merolla

University of Franche-Comté, FEMTO-ST Institute, Besançon, 25000, France

We report on acousto-optical (AO) and electro-optical (EO) LiNbO$_3$ modulators with an active length of only 11 μm. The miniature devices are based on photonic crystal (PhC) structures that are controlled by an external effect (DC electric field or Surface Acoustic Waves). Two processes are presented for realizing the PhCs despite the resistance of the material to etching. The first method is based on direct FIB writing and can yield the fabrication of holes with depth of 3 μm and diameter of 1 μm or less. The second method consists in FIB patterning of a mask which is deposited on the substrate. This process is followed by proton exchange (PE) and reactive ion etching (RIE). Thus, structures with a diameter of 400 nm and an aspect ratio of 3:1 have been fabricated. The methods have been applied to the fabrication of EO and AO micromodulators showing a driving voltage of 13,5 V and a driving electric power of 20 mW respectively. These developments open the way to dense integration of dynamic optical functionalities. [DOI: 10.2971/jeos.2009.09018]

Keywords: scattering loss, sidewall roughness, bent waveguides, silica-on-silicon, indium phosphide

1 INTRODUCTION

Recently, great efforts have been dedicated to the fabrication of tunable photonic crystal (PhC) devices, which offer promising ways of integrating optical functionalities into miniature circuits. Micron-size electro-optical (EO) interferometers or resonators have been demonstrated on silicon substrates, stimulated by the perspective of integrating compact high frequency modulators on miniature circuits for telecommunication systems. [1, 2]. Acousto-optical (AO) micromodulators have also been the subject of recent developments on GaAs or silicon substrates [3, 4] and offer attractive possibilities for the development of new acousto-photonic or photo-phononic devices [5].

Here we propose a new configuration for modulating light, which can be employed for either acousto-optic or electro-optic modulation. It relies on the use of lithium niobate (LiNbO$_3$) substrates. Due to its high electro-optical, acousto-optical and nonlinear coefficients, LiNbO$_3$ represents indeed an excellent candidate for the realization of dynamic PhC structures.

The fabrication of LiNbO$_3$ PhCs represents however a challenging task, due to the well known resistance of the material to standard machining methods. Different approaches have

been conducted for achieving nanostructures with depths larger than 1 μm. Domain engineering followed by wet etching represents a possible way of fabricating submicrometric holes [6], but the method is limited to Z-cut substrates. An alternative relies on ultrafast laser machining [7], but its application to PhCs requires the laser spot to be focused near the diffraction limits. Another common approach consists in preparing the etching of the substrate by modifying the crystal lattice [8]–[13]. Particularly, the method based on proton exchange followed by Reactive Ion Etching (RIE) or Inductively Coupled-Plasma-RIE (ICP-RIE) has shown to be applicable to the fabrication of PhCs [11, 12]. Such a method implies however a consequent number of steps, including the patterning of the mask by electron beam lithography followed by RIE, the proton exchange step and finally the dry etching step. Here we propose to write the patterns directly in the mask by Focused Ion Beam (FIB) milling, which avoids the e-beam lithography and the RIE of the mask. An alternative approach consists in a direct FIB patterning of the substrate [17]. Both methods are suitable for the etching of either X-cut or Z-cut substrates.

The possibility of realizing miniature LiNbO$_3$ components arises with these fabrication methods. Here we show the fea-

sibility of two particular modulators driven by EO or AO effects.

2 THEORY

The proposed devices are schematically depicted in Figures 1 and 2. They consist of a photonic crystal (PhC) integrated on a gradient index optical waveguide. The photonic structure is chosen to be simple (i.e. without any defect), which eases the fabrication processes. The purpose is to exploit the photonic gap in the transmission response of the PhC. More precisely, the PhC is designed so that an edge of the gap corresponds to the operating wavelength. The edge spectral position and consequently the output intensity are dependent on the refractive index. So a periodic array that features gaps in its band structure can become a modulator if it is submitted to an external stimulus (electric field or acoustic wave) that changes the refractive index. The electrodes surrounding the PhC in Figures 1 and 2 are dedicated to the generation of the external stimuli.

The configuration of an electro-optical $LiNbO_3$ modulator has been described in [14], and is reminded in Figure 1(a). The electrodes and the optical waveguide are designed in order to benefit from the highest electro-optic coefficient of the crystal, which is r_{33}. Hence, the electro-optic interaction is optimal if both the electrical and the optical fields are parallel to the Z-axis of the crystal. In the case of an X-cut substrate, the Z axis is in the plan of the substrate, which implies a TE-polarized light wave propagating along the Y axis (see Figure 1(a)). The electric field is made parallel to the Z-axis by coplanar electrodes placed on both sides and parallel to the optical waveguide. The realization of a Z-cut modulator would imply a TM-polarized light, and a push-pull configuration of the electrodes, with the central electrode overlaying the photonic crystal (see Figure 1(b)). Owing to the drift effects, the Z-cut configuration is however less attractive than the X-cut one. Taking for granted that the length of the active section is typically of 11 μm, there is no need of progressive electrodes for achieving large modulation bandwidth.

The basic principle of the acousto-optical modulators is schematically depicted in Figure 2(a). Here the external stimulus is a surface acoustic wave (SAW) generated by an interdigital transducer (IDT) that is placed on one side of the PhC. Due to the piezoelectric interaction in the material, an electric signal applied on the IDT generates a Rayleigh acoustic wave which propagates toward the Z-axis of the crystal. The acoustic wave locally induces a modulation of the refractive index by elasto-optic effect. The effective index of the PhC is modulated provided that the acoustic wavelength is larger than the width of the optical waveguide. The IDT is designed with a period of $p = 9$ μm, which corresponds to an acoustic wavelength of 18 μm. The width of the optical waveguide is of 7 μm. The amplitude of modulation is optimal if it corresponds to the resonance frequency of the IDT which is calculated to be 191 MHz for $p = 9$ μm.

In view of increasing the acousto-optic interaction we propose to exploit a second IDT on the opposite side of the PhC, at the
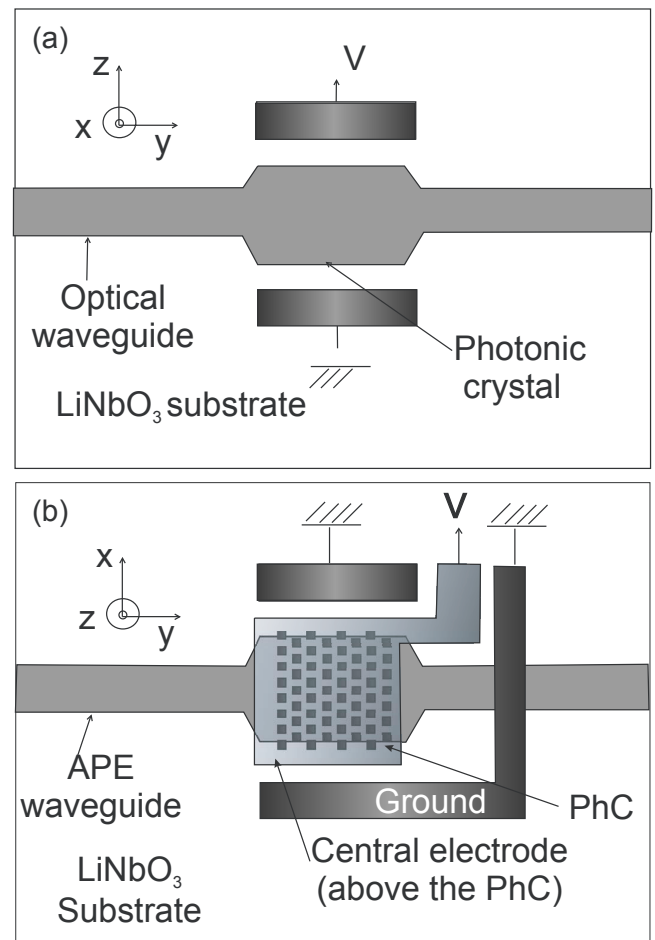

FIG. 1 Basic principle of $LiNbO_3$ electro-optic modulators. (a) X-cut modulator, (b) Z-cut modulator.
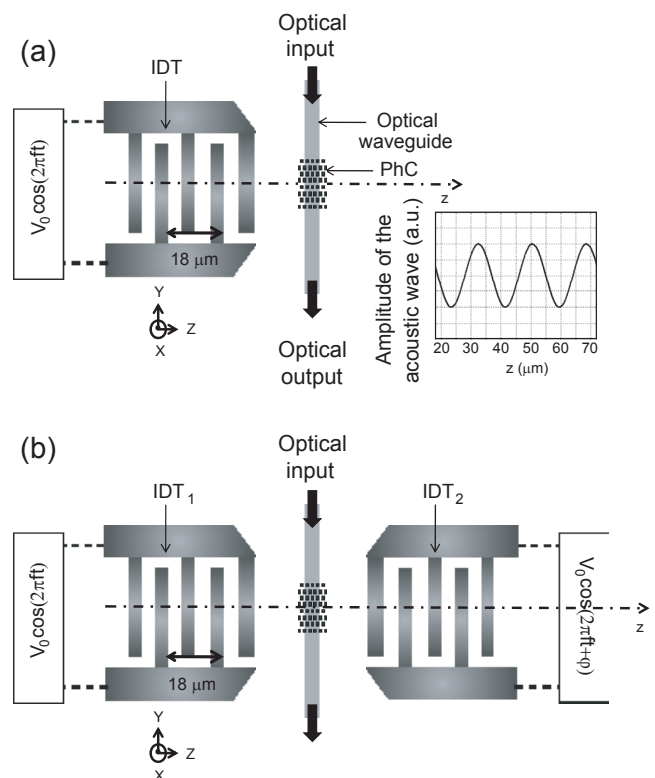

FIG. 2 Schematic of the acousto-optic modulators. (a) Basic principle. (b) Acousto-optic modulator with enhanced acousto-optic interaction.

same distance as the first one (see Figure 2(b)). The second IDT is similar to the first one, and stimulated by the same electric signal. Thus two SAWs are induced with identical amplitudes and frequencies, but with opposite directions of propagation. The interest of the configuration relies on the resulting stationary acoustic wave, which exhibits amplitude twice as large as the one obtained with a single IDT. The modulation amplitude of the output optical intensity depends on the phase between the two applied signals: it is maximal if the phase is equal to zero and minimal if the phase is equal to $90°$.

The first step toward the fabrication of the modulators consists in determining theoretically the optimal geometric parameters of the PhCs. As previously mentioned, we target a simple photonic structure (without any line of defect) featuring a photonic gap. The TE polarization is imposed by the choice of the X-cut substrate and the fabrication process. The gradient index waveguides are indeed achieved by annealed proton exchange (APE), which increases only the extraordinary index of the substrate. We have focused on structures with low group velocity in view of enhancing the optical field in the PhC and increasing the interaction time. The aim is to compensate for the small length of the active section. A quantitative description of the influence of group velocity can be found in [14] for EO devices.

By plane wave expansion (PWE) calculation using the Bandsolve software of Rsoft®, we have determined that a good compromise can be reached between low group velocity, and low radiation losses if the PhC is made of a square array of holes with a ratio of $d/a = 0.5$ between the diameter d of the holes and the period a of the array. Indeed, the fourth band of the band diagram exhibits a flat band edge in the ΓX direction of propagation, as can be observed in Figure 3. The group velocity is deduced from the slope of the band and estimated to be $0,024c$, which is 21 times slower than the group velocity in a regular straight gradient index waveguide. The normalized frequency of the fourth band corresponds to $a/\lambda = 0,55$ where λ denotes the wavelength. So the period will be $a = 825$ nm if the operating wavelength is 1500 nm.
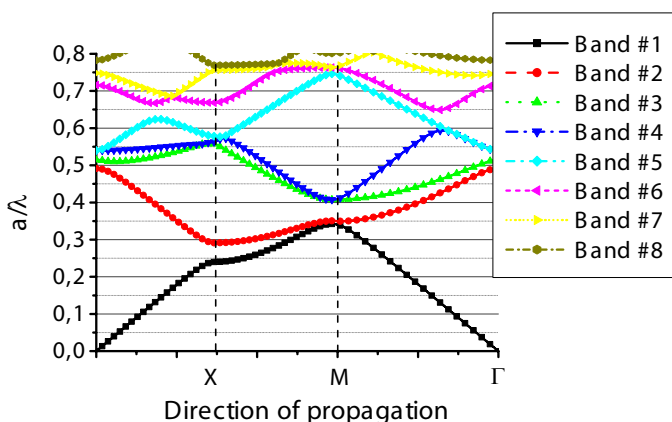

FIG. 3 Band diagram of a square array of holes with diameters of $d = 0,5a$ where a is the lattice period. The calculations were performed by PWE.

By using two-dimensional finite difference time domain (2D-FDTD) homemade calculations, we have determined that a minimal number of rows of 15 is required for obtaining an ex-
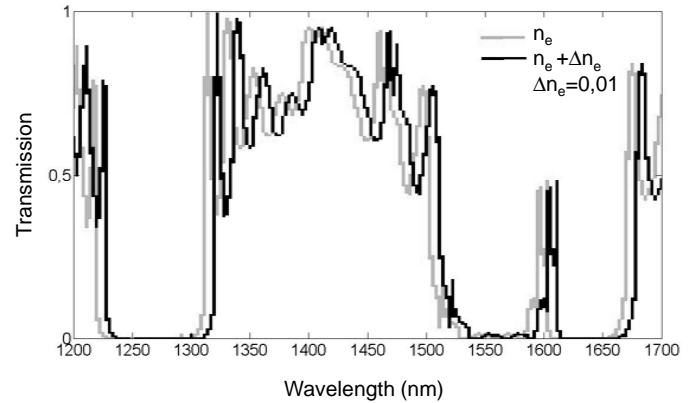

FIG. 4 Theoretical transmission response calculated by 2D-FDTD method for a 15 × 15 square array of holes with a period of 825 nm and a hole diameter of 412 nm. Gray line: transmission response through the PhC without external stimulus. Black line: expected transmission response for an induced variation of the refractive index of 0.01.

tinction ration better than $−13$ dB. Details about the FDTD-2D calculations are provided in [19]. The resulting transmission response is reported in Figure 4 with (black line) and without (gray line) an external stimulus. A shift of 7 nm is expected in the transmission spectrum if the refractive index is submitted to a variation of 0.01. In a regular straight optical waveguide, this refractive index variation would imply an unacceptable driving power, corresponding to an 863 V applied voltage for the EO devices or to an acoustic power of 2 W for the AO devices (see [14] and [15] for more details on the calculations of the driving powers). We are going to see in Section 4 that the required external driving power is significantly reduced owing to slow light effects in the PhC.

3 FABRICATION

The chips are fabricated on a 0.5 mm thick X-cut LiNbO$_3$ wafer. The optical gradient index waveguide is realized in a first step by annealed proton exchange (APE). This step is achieved through a SiO$_2$ mask in benzoic acid at $180°$C for 1.5 hours. The process is followed by an annealing of the optical waveguide at $333°$C for 9 hours. The parameters are chosen in order to make the optical core as close as possible to the surface while keeping an electro-optic coefficient of 30 pm/V at 1.55 μm wavelength. With such experimental parameters, the optical core is estimated to be at 1.4 μm from the surface, which can be compared to the 3 μm depth that would result from a standard Ti-diffusion process. The electrodes are sputtered onto the surface in a second step. Capacitive Ti electrodes are deposited with a thickness of 200 nm for EO devices, while Al IDTs are designed with a thickness of 200 nm for AO devices.

The key fabrication step is the etching of the PhCs. In what follows, we are going to show two methods that were developed for the fabrication of the LiNbO$_3$ PhCs.

3.1 Fabrication of lithium niobate photonic crystals by direct FIB milling

The first method relies on direct FIB patterning of the substrate. This method was firstly employed by S. Yin et al. to etch submicrometric 1D LiNbO$_3$ structures in 1999 [16]. In [17], we have extended the method to the fabrication of 2D PCs with depth of 2 μm. The method begins with the sputtering of a Cr layer with a thickness of 15 nm on to the substrate. The substrate is then introduced into the FIB chamber and exposed to a Ga$^+$ liquid metal ion source (LMIS) with ion acceleration energy of 30 keV. The pseudo-Gaussian shaped spot size is estimated to be 40 nm on the target. Multiple exposures are mandatory to avoid redeposition of the material in the neighborhood. Typically, the achievement of a hole with a width of 400 nm and a depth of 2 μm requires fifty loops. The dwell time is 0.5 ms, the step size is 11.4 nm and the total exposure time is typically 2 hours for a 15 $\times$ 15 array of holes. With this method, we have managed to obtain matrices with holes as small as 110 nm (see Figure 5(a)), and depth larger than 1 μm. A few realizations are shown in Figure 5. Figure 5(a) shows a triangular array of 5 $\times$ 5 holes with a depth of 1.5 μm and a diameter of 330 and 110 nm respectively. In Figure 5(b), we can see that depths of 2 μm can be reached when the period is of the order of 1 μm. The conical shape seen in the image is intrinsic to the method, and cannot be improved, unless by using additional gases that would help removing Nb from the etched substrate. In [14] and [18], some of the authors have demonstrated that photonic bandgap structures could be obtained with this method, despite the conical shape of the holes.

3.2 Fabrication of lithium niobate PhCs by FIB milling followed by RIE etching

A second method based on PE and RIE has been developed to reduce the fabrication time linked to the FIB process, and to fight against the conical shape of the holes. Indeed, the fabrication of 100 $\times$ 50 holes would require 44 hours of total FIB exposure, which is unacceptable. The first step of the second method consists in sputtering a 650 nm thick layer of polysilicon onto the substrate. The sample is then introduced into the FIB vacuum chamber. The parameters for etching are the same as previously described, but the dwell time is reduced to 0.2 ms, and the number of exposure is now of 30. A cross section of the polysilicon mask after FIB milling can be seen in Figure 6(a).

The method is followed by proton exchange (PE) in molten benzoic acid at 190°C. This step is essential to produce a significant lattice deformation which facilitates the etching step to come. Moreover, the replacement of Li$^+$ ions with H$^+$ ions helps preventing from LiF redeposition during the etching step, which plays a role in both the verticality of the substrate and the etch-rate. The pattern is then transferred to the substrate by CHF$_3$ RIE etching with a Plassys reactor. In order to enhance the chemical aspect of the RIE etching, we work with CHF$_3$ at pressures of 25-100 μbar, and RF power levels of 50-150 W.

The role of each parameter is detailed in [12]. After two hours of RIE at 100 W RF power and 60 μbar operated pressure, we
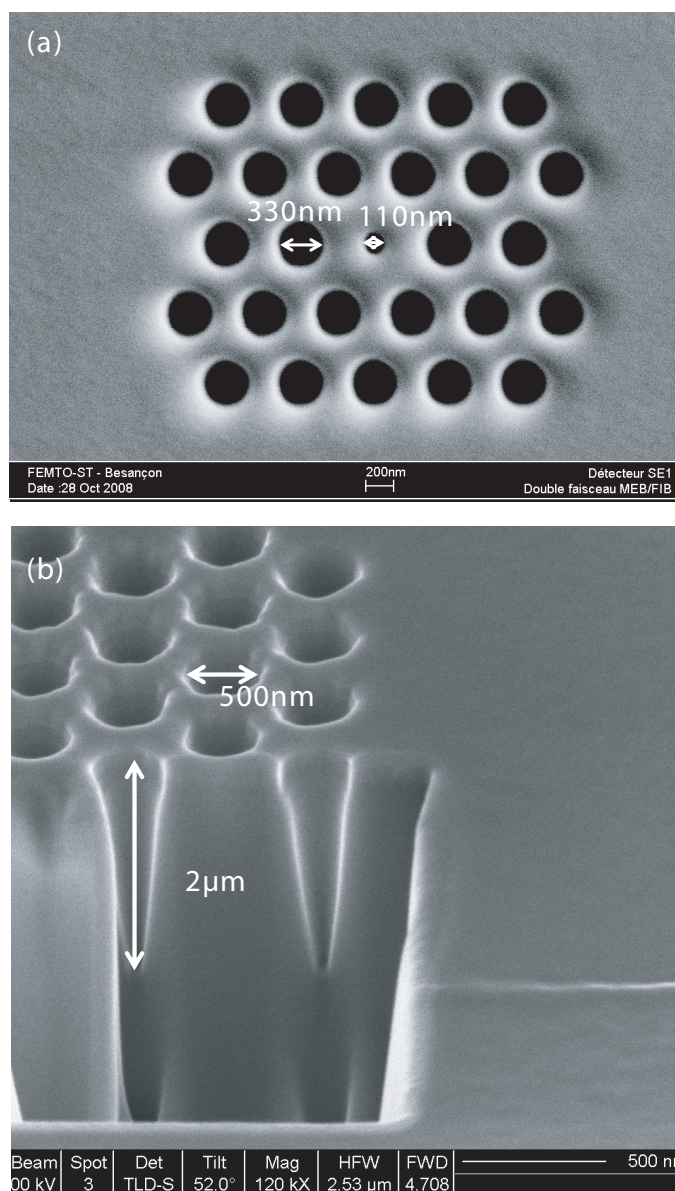
FIG. 5 SEM views of LiNbO$_3$ photonic crystals fabricated by FIB milling. (a) Triangular arrangement of 5 $\times$ 5 holes with a diameter of 130 nm and a center hole of 110 nm. (b) FIB cross section of a triangular arrangement of 4 $\times$ 4 holes with diameter of 500 nm, and depth of 2 μm, tilt = 52°.

have achieved matrices of holes with a diameter of 420 nm diameter and a depth of 1.2 μm (see Figure 6(b)). The side wall verticality is of the same order as that achieved by direct FIB patterning, but it should be improved by replacing the RIE step with an ICP-RIE step, which is currently under test. With such parameters, the total exposure time for a matrix of 100 $\times$ 50 holes is reduced to 10 hours for the FIB exposure, in addition to the 6.5 hours of proton exchange and 2 hours of RIE etching. Thus, the total duration of the process is 19 hours that can be advantageously compared with the 44 hours associated with direct FIB milling. This method is currently under test for the fabrication of photonic bandgap structures.

Demonstrators of EO and AO micromodulators were fabricated by direct FIB milling. The detail of the characterization of EO modulators has been reported elsewhere [14]. Here we report the main associated results and detail how the actual performances of EO micromodulators can be improved. A sec-
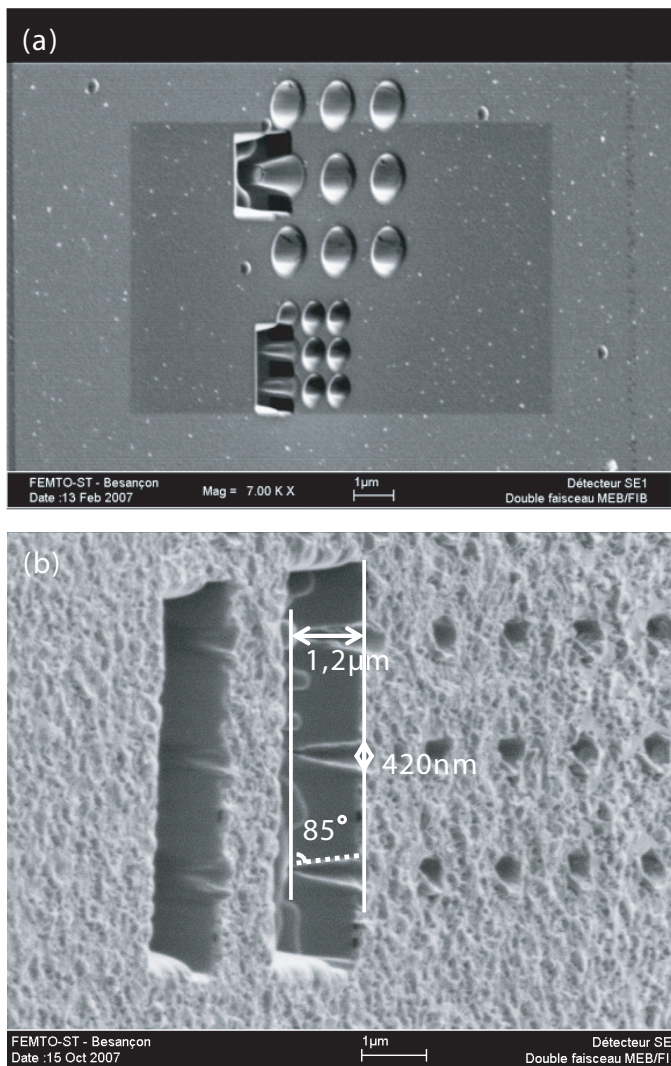
FIG. 6 SEM images of patterns, tilt = 50°. (a) Cross-view of the polysilicon mask af-
ter FIB milling. (b) Image of an X-cut substrate after etching of the Si mask layer,
and 120 min of RIE etching. Pressure = 60 μbar – Power = 100 W – Resulting
depth = 1.2 μm.

ond subpart is dedicated to the characterization of AO modu-
lators.

4 CHARACTERIZATION OF THE MODULATORS

4.1 Electro-optical modulators

An overview of the electro-optical structures is given in Fig-
ure 7: the component is connected to a DC power supply via
a printed circuit board (PCB) and wire bonding.

The resulting experimental large spectrum transmission is
represented in Figure 8, while Figure 9 shows the figure of
modulation at a wavelength of 1286 nm. These results demon-
strate experimentally that an applied voltage induces a shift
of 5 nm/V. The sign of the wavelength shift depends on the
sign of the applied voltage, which shows that the modula-
tion is due to an electro-optical effect, rather than to a thermo-
optical effect. The driving voltage is measured to be 13.5 V,
and the extinction ratio is of 5.2 dB (see Figure 9) at a wave-
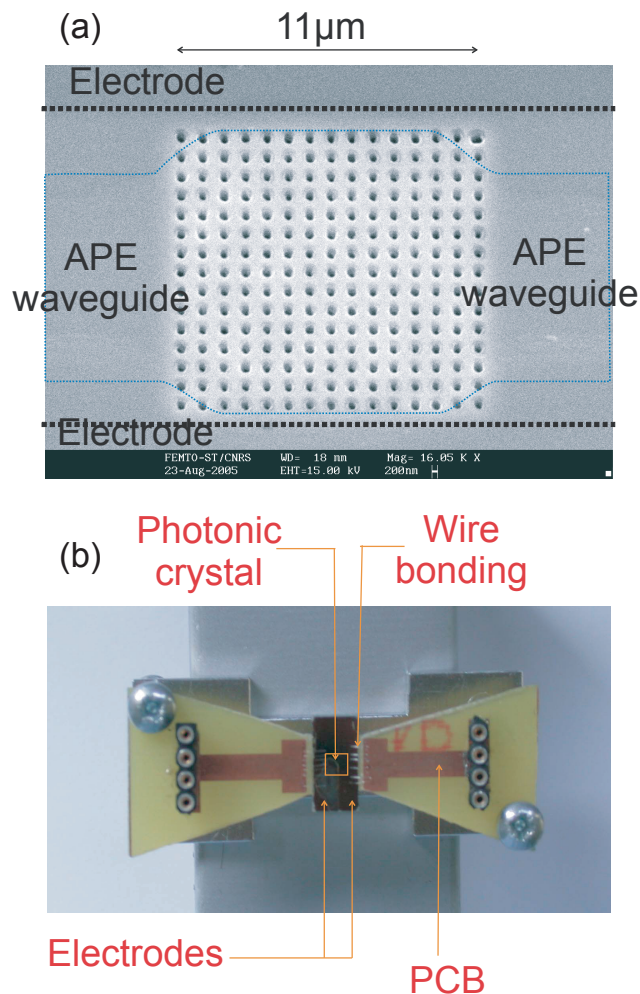

FIG. 7 Electro-optic photonic crystal modulators. (a) SEM view of the photonic crystal.
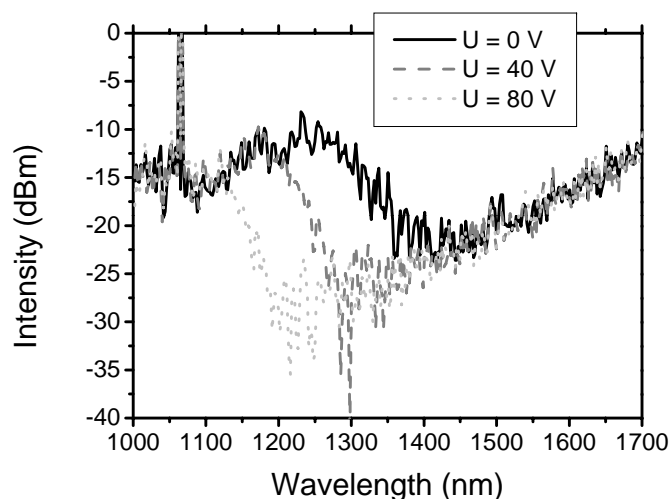(b) Picture of the connected PC modulator.

FIG. 8 Measured transmission of the photonic crystal for different applied external
voltages (0, 40, and 80 V).

length of 1286 nm. These results confirm the significant role
of low group velocity for reducing the driving power. Indeed,
the calculations led to a shift of 7 nm for 863 V (that is 8 pm/V)
for a regular optical waveguide. The experimental shift of
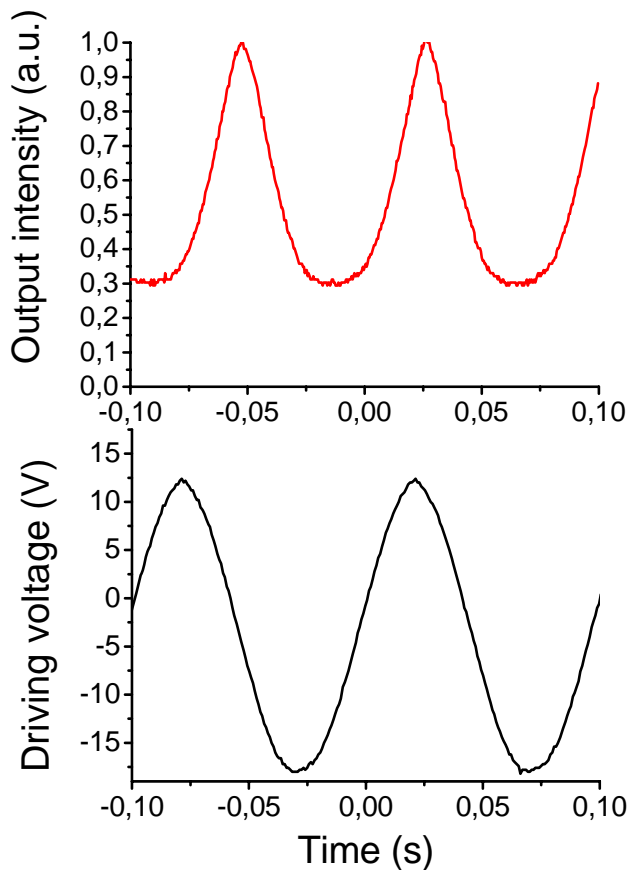5 nm/V demonstrates that the employment of low group ve-

FIG. 9 Figure of modulation at 1286 nm for an optical input power of 1 mW. Top: optical response at the output of the modulator. The output intensity is represented relatively to the maximum output intensity. Bottom: driving voltage.

locity helps reducing more than 100 times the device driving voltage.

The measured bandwidth is 500 MHz, but it can be enlarged with an appropriate circuit. Indeed, the picture of Figure 7 clearly shows that the PCB circuit and the electrodes are not optimized for high bandwidth modulation and low driving voltage. More precisely, the use of a matched PCB with K connectors should help improving consequently the bandwidth. Further improvement of the bandwidth can be reached by reducing the capacity of the electrodes, which is measured to be $C_0 = 6.2$ pF. This capacity can be reduced to $C_1 = C_0 \cdot L_1/L_0$ if the length of the electrodes is reduced from $L_0 = 1$ cm to $L_1 = 11$ μm, which are respectively the actual length of the electrodes and the length of the PhC. With reduced electrodes, the bandwidth will be increased from $f_0 = 1/(2\pi R \cdot C_0)$ to $f_1 = f_0 \cdot L_1/L_0 = 450$ GHz. This limit can even be increased to THz by lowering the effective dielectric permittivity of the device with a ridge structure or a thin substrate.

The slope of the edge gap is one of the most important parameters that influence the driving voltage. The actual demonstrator exhibits a slope of 0.15 dB/nm in the transmission response, which means that a shift of 70 nm of the spectrum induces a variation of -10.5 dB of the transmission response at the operating wavelength of 1300 nm. Such experimental parameters should be dramatically improved by enhancing the slope of the edge gap. The 2D-FDTD calculations of the trans-

mission response allow estimating that the maximum reachable slope with such a structure is 0.8 dB/nm. If this limit were reached, the driving voltage would be reduced by a factor of 5. We will see in Section 4.2 that an improvement of the aspect ratio of the holes enables a consequent improvement of the gap slope.

4.2 Acousto-optical modulators

An SEM image of the AO modulators can be visualized in Figure 10. The acoustic aperture of the IDTs is of 400 μm, and their configuration has been studied for reducing capacitive effects. They are wire bonded to a PCB which is itself connected to SMA wires via SMA connectors. The PCB is designed for ensuring impedance matching. The electric transmission (s_{21}) and reflection (s_{11}) through the IDTs were measured with a ZVRC vector network analyzer (Rhode & Schwarz). The results are reported in Figures 11(a) and (b) respectively. From these measurements, we can deduce that the resonance frequency is confirmed to be 191 MHz, and that the maximum of transmission through the connected IDTs is be -6.5 dB. The minimum of reflection corresponds to -32 dB. So 47% of the electric input power is converted into acoustic power at the frequency of resonance of the IDT.
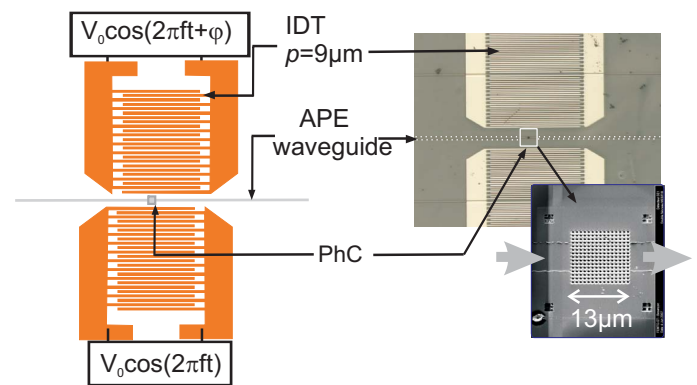

FIG. 10 Acousto-optical PhC modulators. Lefts: scheme of the device. Rights: photograph of the IDTs (20x), and SEM view of the photonic crystal surrounded by the IDTs.

The optical spectrum through the PhC was measured with a supercontinuum source as described in [14]. An extinction ratio of -30 dB is achieved (see Figure 12), which is due to an improvement of the nanostructuration since the fabrication of the EO modulators. The acousto-optic characterization was performed with a DFB laser diode emitting at 1400 nm wavelength. The laser light was injected into the optical waveguide on which was written the PhC. A high frequency generator (HF) was employed for generating a sinusoidal signal with a power of 13 dBm and a frequency of 191 MHz. The electric signal was divided in two signals by a delay line. Each of the two outputs of the delay line was connected to an IDT. Thus, the delay line enabled a control of the phase between the two signals applied on the IDTs. The maximum of modulation is achieved for a phase equal to zero between the two IDTs, and at the resonance frequency of the IDT. The two applied signals and the resulting modulation in these conditions are shown in Figures 13(a) and (b) respectively. It can be seen in Figure 13(a) that the delay line induces a slight difference between the two

(a)

FIG. 12 Optical transmission through a single APE waveguide (dashed line), and through an APE waveguide realized in the same conditions, on which is written a square array of 15 × 15 holes (solid line) with a period of 826 nm and a diameter of 413 nm
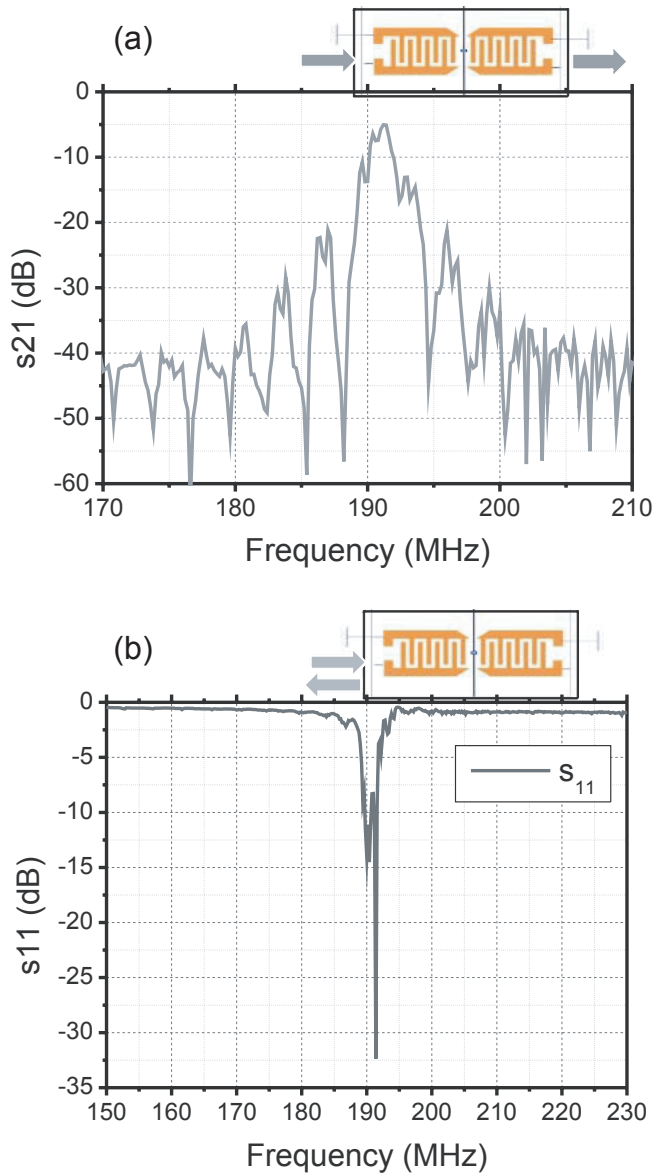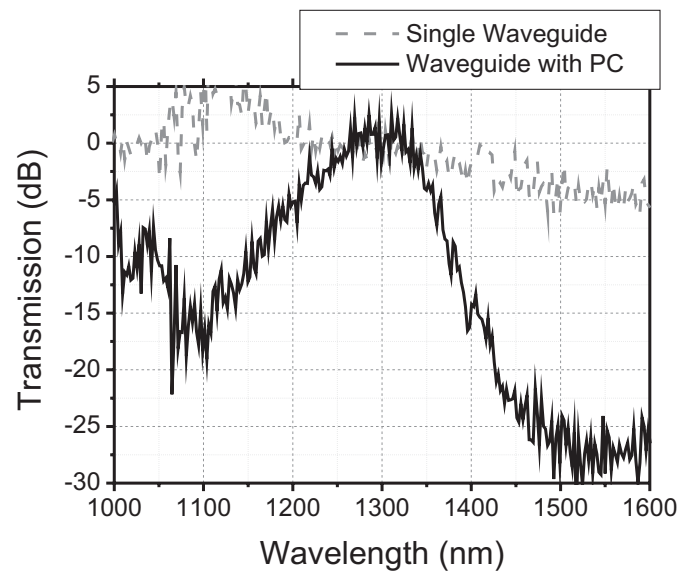
(b)

FIG. 11 Electrical characterization of the IDTs. (a) Transmission, (b) Reflection.

voltages applied on the IDTs. The extinction ratio is estimated to be -5.4 dB at 191 MHz for a driving power of 13 dBm (20 mW) (see Figure 12(b)). The corresponding acoustic power is evaluated to be 9 mW.

The amplitude of modulation is maximal at 191 MHz and decreases all the more than the operating frequency differs from the frequency of resonance of the IDT. If a thermo-optic effect or an electro-optic effect were responsible for the modulation, its amplitude would not depend on frequency. Consequently, these results demonstrate that the modulation is due to an acousto-optic effect.

5 CONCLUSION

We have demonstrated the feasibility of LiNbO$_3$ AO and EO micromodulators, and developed two methods for nanostructuring LiNbO$_3$ substrates. The two methods are well-suited for the fabrication of holes with diameter as small as 180 nm, for either X-cut or Z-cut substrates. Aspect ratios of 3:1 or more have been achieved with both methods. The first
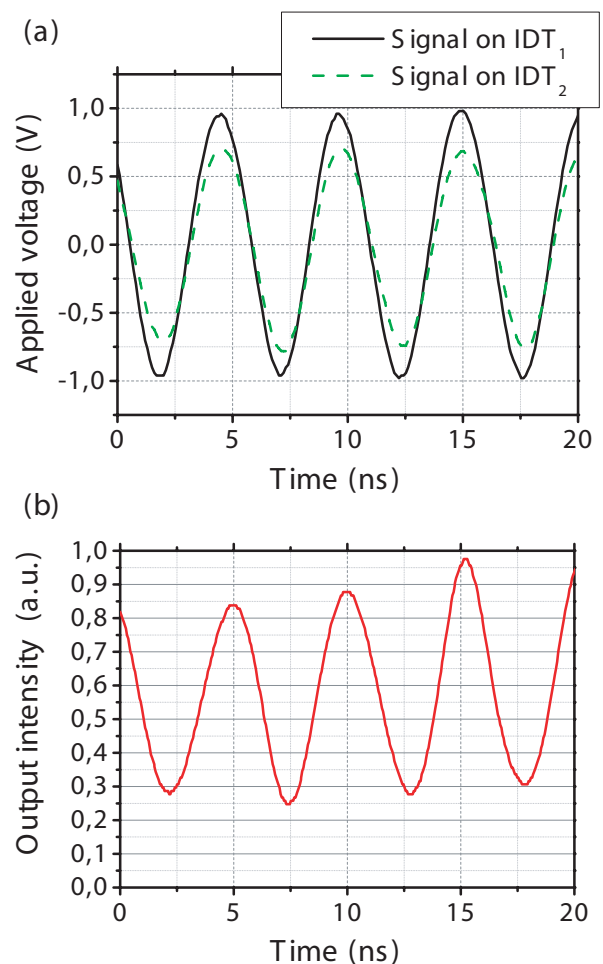
(a)

(b)

FIG. 13 Acousto-optic characterization of the micromodulators at 191 MHz frequency. (a) Electric signals applied on the IDTs. (b) Resulting intensity modulation at the output of the optical waveguide.

method, based on direct FIB patterning, is adequate for fields of photonic crystals smaller than 50×50 μm^2. The second method implies using the FIB as a lithographic tool that pat-

terns a polysilicon mask. In this case, subsequent steps of proton exchange and CHF$_3$ RIE are required. This method shows out to be interesting for structures exhibiting more than 500 holes. The methods enable the fabrication of new miniature modulators, with active length of only 11 μm. An EO modulator with a driving voltage of 13.5 V and an AO modulator with a driving power of 20 mW have been demonstrated. Further improvements can be reached by optimizing the capacitive electrodes of the EO modulator, and by achieving a better side wall verticality of the nanostructures. Appealing perspectives of fabricating miniature dynamic optical circuit can arise with these developments.

ACKNOWLEDGMENTS

References

[1] L. Gu, W. Jiang, X. Chen, L. Wang, and R. T. Chen, "High speed silicon photonic crystal waveguide modulator for low voltage operation" Appl. Phys. Lett **90**, 071105 (2007).

[2] B. Schmidt, Q. Xu, J. Shakya, S. Manipatruni, and M. Lipson, "Compact electro-optic modulator on silicon-on-insulator substrates using cavities with ultrasmall modal volumes" Opt. Express **15**, 3140–3148 (2007).

[3] P. D. Batista, B. Drescher, W. Seidel, J. Rudolph, S. Jiao, and P. V. Santos, "ZnO/SiO2 microcavity modulator on silicon" Appl. Phys. Lett. **92**, 133502 (2008).

[4] M. M. de Lima, Jr., R. Hey, and P. V. Santos, "Active photonic crystals based on surface acoustic waves" Appl. Phys. Lett. **83**, 2997–2999 (2003).

[5] V. Laude, M. Wilm, S. Benchabane, and A. Khelif, "Full bandgap for surface acoustic waves in a piezoelectric phononic crystal" Phys. Rev. E **71**, 036607 (2005).

[6] P. Ferraro and S. Grilli, "Modulating the thickness of the resist pattern for controlling size and depth of submicron reversed domain in lithium niobate" Appl. Phys. Lett. **89**, 133111 (2006).

[7] D.W. Ward, E.R. Statz, and K.A. Nelson, "Fabrication of polaritonic structures in LiNbO$_3$ and LiTaO$_3$ using femtosecond laser machining" Appl. Phys. A-Mater. **86**, 49–51 (2007).

[8] F. Laurell, Jonas Webjörn, G. Arvidsson, and J. Holmberg, "Wet etching of proton exchanged lithium niobate-a novel processing technique" J. Lightwave Technol. **10**, 1606–1610 (1992).

[9] T.-J. Wang, C.-F. Huang, W.S. Wang, and P.-K. Wei, "A novel wet-etching method using electric-field-assisted proton exchange in LiNbO$_3$" J. Lightwave Technol. **22**, 1764–1767 (2004).

[10] D.M. Gill, D. Jacobson, C.A. White, D.W. Jones, Y. Shi, W. J. Minford, and A. Harris, "Ridged LiNbO$_3$ modulators fabricated by a novel oxygen-ion implant/wet-etch technique" J. Lightwave Technol. **22**, 887–890 (2004).

[11] H. Hu, A.P. Milenin, R.B. Wehrspohn, H. Hermann, and W. Sohler, "Plasma etching of proton-exchanged lithium niobate" J. Vac. Sci A **24(A)**, 1012–1015 (2006).

[12] G. Ulliac, N. Courjal, H. M.H. Chong, and R.M. De La Rue, "Batch process for the fabrication of LiNbO$_3$ photonic crystals using proton exchange followed by CHF$_3$ reactive ion etching" to be published in Opt. Mater. R3591 (2009).

[13] Z. Ren, P.J. Heard, J.M. Marshall, P.A. Thomas, S. Yu, "Etching characteristics of LiNbO$_3$ in reaction ion etching and inductively coupled plasma" J. Appl. Phys. **103**, 034109 (2008).

[14] M. Roussey, M.-P. Bernal, N. Courjal, D. Van Labeke, F. I. Baida and R. Salut, "Electro-optic effect exaltation on lithium niobate photonic crystals due to slow photons" Appl. Phys. Lett. **89**, 241110 (2006).

[15] V. Laude, M. Wilm, and S. Ballandras, "Least action principle for the estimation of the slowness and the attenuation of pseudo surface acoustic waves" J. Appl. Phys. **93**, 10084 (2003).

[16] S. Yin, "Lithium niobate fibers and waveguides: fabrication and applications" Proc IEEE **87**, 1962–1974 (1999).

[17] F. Lacour, N. Courjal, M.P. Bernal, A. Sabac, C. Bainier, M. Spajer, "Nanostructuring lithium niobate substrates by focused ion beam milling" Opt. Mater. **27**, 1421–1425 (2005).

[18] M.-P. Bernal, N. Courjal, J. Amet, M. Roussey, C.H. Hou, "Lithium niobate photonic crystal waveguides: far field and near field characterization" Opt. Commun. **265**, 180–186 (2006).

[19] M. Roussey, M.-P. Bernal, N. Courjal, and F. I. Baida, "Experimental and theoretical characterization of a lithium niobate photonic crystal" Appl. Phys. Lett. **87**, 241101 (2005).